Vanadium oxide nanostructures: from zero- to three-dimensional

2006 J. Phys.: Condens. Matter 18 R1

(http://iopscience.iop.org/0953-8984/18/4/R01)

INSTITUTE OF PHYSICS PUBLISHING JOURNAL OF PHYSICS: CONDENSED MATTER

J. Phys.: Condens. Matter **18** (2006) R1–R14 doi:10.1088/0953-8984/18/4/R01

TOPICAL REVIEW

Vanadium oxide nanostructures: from zero- to three-dimensional

J Schoiswohl[1], S Surnev[1], F P Netzer[1] and G Kresse[2]

[1] Institut für Physik, Oberflächen- und Grenzflächenphysik, Karl-Franzens-Universität Graz, A-8010 Graz, Austria
[2] Institut für Materialphysik, Universität Wien, A-1090 Wien, Austria

Received 16 November 2005, in final form 6 December 2005
Published 9 January 2006
Online at stacks.iop.org/JPhysCM/18/R1

Abstract

Oxide structures with nanometric dimensions exhibit novel physical and chemical properties, with respect to bulk oxide materials, due to the spatial confinement and the proximity of the substrate. They derive their atomic structure and morphology, on the one hand, from the interactions at the interface between the oxide overlayer and the substrate and, on the other hand, from kinetic constraints during the growth process. Here we describe the formation of vanadium oxide nanostructures on a single-crystal metal surface and their characterization by scanning tunnelling microscopy (STM) and *ab initio* density functional theory (DFT) calculations. We show that vanadium oxide nanostructures can be formed on Rh(111) with morphologies ranging from quasi-zero- to three-dimensional and that the oxide growth can be tuned into a particular dimensionality by careful adjustment of experimental parameters. These 'artificial oxide phases' display new physical and chemical properties, which make them potentially interesting materials for nanotechnology applications.

(Some figures in this article are in colour only in the electronic version)

Contents

1. Introduction 2
2. Preparation and characterization of vanadium oxide nanostructures 3
3. Vanadium oxide nanolayer phases 4
4. Planar vanadium oxide clusters (0D oxide nanostructures) 9
5. 1D oxide nanostructures 11
6. 3D oxide nanoparticles 12
7. Synopsis 13
Acknowledgments 14
References 14

1. Introduction

Vanadium oxides belong to the important class of early 3d transition metal compounds [1] which have received considerable attention in research and technology over the last decades. In bulk form, vanadium oxides display different oxidation states and V–O coordination spheres and exhibit a broad variety of electronic, magnetic and structural properties [2, 3] which make these materials attractive for many industrial applications. Prominent examples range from the area of catalysis, where vanadium oxides are used as components of important industrial catalysts for oxidation reactions [4] and environment pollution control [5], to optoelectronics, for the construction of electrical switching devices [6] and smart thermochromic windows.

When the dimensionality of oxide materials is reduced, new properties, either local or collective, may appear. Nanometric oxide structures in the form of ultrathin layers, line elements, quantum dots and three-dimensional clusters are of significant importance as passive and active elements in different areas of the emerging nanotechnologies. Examples comprise electronic, optoelectronic and magneto-electronic device technology, sensing devices, heat- and corrosion-resistive coatings or the field of advanced catalysis. In all these areas the controlled fabrication of nanostructured oxide phases is required.

In view of the importance of vanadium oxides in different technological applications, the fabrication of this material in nanostructured form is a particularly attractive goal. For example, in the field of solid-state electrochemistry, nanocomposites of vanadium pentoxide (V_2O_5) in combination with conducting polymers have been designed as cathode material for rechargeable Li^+ batteries [7]. Recently, vanadium oxide nanotubes and nanowires [8] with a diameter in the range of 15–150 nm have been produced by sol–gel synthesis, and such strongly anisotropic materials are of particular interest in the electrochemistry and catalysis; in particular VOx nanotubes are considered as promising nanoscale electrodes for Li^+ batteries [9]. In a different area, ultrathin films of VO_2 are used as optical and electrical switching devices [10]. The underlying physical property is the metal–insulator transition in VO_2 at 68 °C, with the associated dramatic changes in the optical transmission and electrical resistance.

In order to exploit the full technological potential of vanadium oxide nanostructures a detailed knowledge of their properties at the atomic scale is necessary. A possible approach to tackle this problem is the fabrication of ultrathin oxide films on single-crystal metal substrates by physical vapour deposition. In this article we review the preparation of structurally well-defined vanadium oxide nanostructures on a metal surface and their characterization by scanning tunnelling microscopy and density functional theory calculations. As a prototypical metal substrate the Rh(111) surface will be discussed. By choosing suitable oxide preparation techniques (reactive evaporation versus post-oxidation or post-deposition) and the proper thermodynamic parameters (oxygen pressure, evaporation rate and substrate temperature), we find that four different types of vanadium oxide nanostructures can form on the rhodium substrate. These include:

(i) molecular oxide clusters with dimensions <1 nm, which can be considered as zero-dimensional (0D) nanostructures;
(ii) elongated oxide islands with a width of only a few unit cells and an aspect ratio of $\sim$10, which represent quasi-one-dimensional (1D) structures;
(iii) ultrathin oxide layers with a thickness of less than 1 nm or two-dimensional (2D) nanolayers, and
(iv) three-dimensional (3D) oxide nanoparticles, with an average size of less than 10 nm.

Despite the fact that the geometry of the four types of oxide structures is different, there exist some common features. The low-dimensional oxide phases form spontaneously on the

Rh(111) surface and are stabilized by the interaction with the latter. Most of them exhibit novel structures, which are not known in the bulk form. These oxide phases can be considered as artificial materials, which are constructed by common building units, containing V–O coordination spheres, which are different from those of bulk-type vanadium oxides. By careful adjustment of thermodynamic parameters, such as the temperature, the vanadium coverage or the chemical potential of oxygen, the V–O building blocks can be organized into different structures and this allows one to control the design of oxide nanostructures on the metal surface.

2. Preparation and characterization of vanadium oxide nanostructures

In order to fabricate oxide nanostructures of various dimensionalities and a high degree of structural order it is essential to balance the thermodynamic and kinetic forces that drive the chemistry and the mass transport associated with the formation of the oxide layer, particularly when the metal of interest exhibits a large range of oxidation states, as does vanadium. The thermodynamic forces are given by the materials chosen and include the surface and interface energies of the metal (oxide) surface and the oxide–metal interface, whereas the kinetic effects can be adjusted by varying the experimental deposition parameters, such as substrate temperature, oxygen pressure and evaporation rate.

The vanadium oxide nanostructures considered in this article have been grown by physical vapour deposition (PVD) onto atomically clean Rh(111) single-crystal metal surfaces. Three different kinetic routes were used for the preparation of the nanostructures. In the *reactive evaporation* (RE) method vanadium metal was evaporated in an oxygen atmosphere (at typically $p(O_2) = 2 \times 10^{-7}$ mbar) onto the clean metal substrate, kept at elevated temperature (up to 400 °C) to provide the mobility necessary to obtain a high degree of structural order in the oxide overlayer. To prevent oxide reduction or decomposition following the vanadium deposition the sample was cooled down to room temperature in an oxygen atmosphere. In our studies vanadium was evaporated from an electron beam evaporator (Omicron) and the deposition rate was monitored by a quartz crystal microbalance; a rate of 0.2 monolayer min^{-1} was typically employed. The vanadium oxide coverage is given in monolayer equivalents (MLE), where 1 MLE contains the same number of vanadium atoms as one monolayer of Rh(111) atoms. Alternatively, the *post-oxidation* (*PO*) method was used, which consists of deposition of vanadium in ultra-high vacuum (UHV) onto the metal substrate, kept at room temperature to prevent a possible alloying with the vanadium metal. Subsequently the vanadium layer was oxidized by heating the sample in an oxygen atmosphere. For the generation of 0D and 1D oxide nanostructures a third technique, called *post-deposition* (*PD*), was employed, where the metal substrate is initially pre-covered by a layer of chemisorbed oxygen, the amount of which is known (for example, the O(2 × 1) chemisorbed phase on Rh(111) contains 0.5 ML oxygen atoms) and these oxygen species serve as a reservoir for the subsequent oxidation of vanadium. Metallic vanadium is deposited onto this surface in UHV at room temperature and is followed by a flash to typically 250 °C to lower the reaction barrier for the vanadium oxidation.

Variable-temperature scanning tunnelling microscopy (STM) was the main instrumental tool for the characterization of the morphology and the atomic structure of the vanadium oxide nanostructures. The experiments were carried out in a custom-designed UHV system with a typical base pressure of 5×10^{-11} mbar, described elsewhere [11]. To model the structure of the various low-dimensional vanadium oxide phases density functional theory (DFT) calculations were performed using the Vienna *ab initio* simulation package (VASP), as described in more detail in [12, 13].

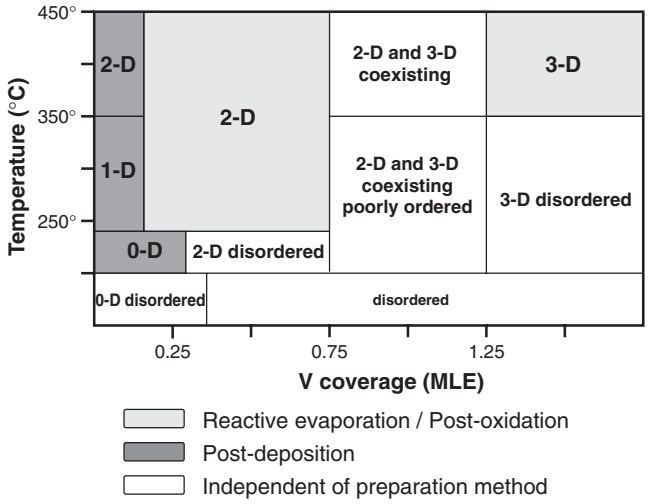

Figure 1. Phase diagram of vanadium oxide nanostructures on Rh(111) as a function of the vanadium coverage and the substrate temperature.

Figure 1 shows a phase diagram of the vanadium oxide/Rh(111) system in terms of different oxide structures with reduced dimensions, as a function of the oxide preparation method, the vanadium oxide coverage (horizontal axis) and the substrate temperature (vertical axis) during the evaporation or annealing. The phase diagram was derived on the basis of topographic STM images, which are summarized in figure 2. Deposition of small (<0.2 ML) amounts of vanadium metal onto the Rh(111) surface pre-covered with oxygen (post-deposition method), followed by a low-temperature (<250 °C) flash, results in the formation of isolated molecular oxide clusters (figure 2(a)) with lateral dimensions of ∼1 nm and a height of 0.1 nm, which can be considered as 0D oxide nanostructures. Increasing the mobility of these oxide clusters by applying higher temperatures (up to 250 °C) during the flash annealing causes their aggregation into oxide islands (figure 2(b)), which are elongated along the main azimuthal directions of the substrate. These quasi-1D objects exhibit an aspect ratio of up to 10, but they are only kinetically stabilized on the Rh(111) surface and transform into more isotropic 2D islands when annealed to higher temperatures. In a relatively broad range of coverage (0.2–0.8 MLE) the 2D morphology is the dominating oxide growth mode (figure 2(c)). Both RE and PO methods are equally well suited to the preparation of such 2D oxide nanostructures. At oxide coverages exceeding 1 MLE the oxide growth mode changes from 2D to 3D. This is illustrated in figure 2(d), where regularly shaped 3D vanadium oxide islands with a height of ∼2 nm decorate the Rh(111) steps. Here as well, the RE and PO methods and substrate temperatures above 350 °C are the preferred procedures since they yield the best ordered structures. We will focus here only on those regions of the phase diagram at which homogeneous and atomically well ordered vanadium oxide nanostructures can be generated (highlighted regions in figure 1). We begin the discussion with the 2D vanadium oxide layers on Rh(111), which are of key importance for understanding the 0D and 1D oxide nanostructures.

3. Vanadium oxide nanolayer phases

Ultrathin oxide layers supported on metal substrates may exhibit novel physical and chemical properties that are not shared by their respective bulk counterparts. These so-called *oxide*

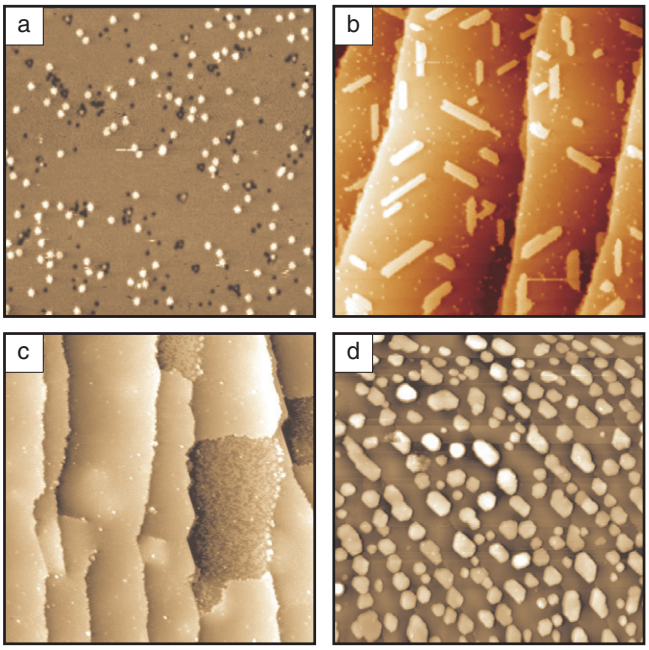

Figure 2. Constant current topographic STM images of (a) 0D (47 × 47 nm^2, $U = +2.0$ V, $I = 0.2$ nA), (b) 1D (140 × 140 nm^2, $U = +2.0$ V, $I = 0.1$ nA), (c) 2D (100 × 100 nm^2, $U = +2.0$ V, $I = 0.1$ nA) and (d) 3D (200 × 200 nm^2, $U = +2.0$ V, $I = 0.1$ nA) vanadium oxide nanostructures.

nanolayers derive their stability from the interactions at the interface to the metal substrate and from the 2D confinement; they can be regarded as artificial oxide phases with new structures that do not occur in nature [14]. The vanadium oxide/Rh(111) system is particularly rich in this respect, since it shows a large diversity of ordered 2D oxide phases, with morphologies, structures and stoichiometries that can be controlled by the oxygen pressure and the substrate temperature [12, 15].

Under highly oxidative conditions, i.e. $p(O_2) = 2 \times 10^{-7}$ mbar, $T_{substrate} = 400\,^{\circ}$C, a vanadium oxide layer with a $(\sqrt{7} \times \sqrt{7})$R19.1° structure (called $\sqrt{7}$ hereafter) forms [15]. At low submonolayer coverages ($\Theta < 0.3$ MLE) the $\sqrt{7}$ layer grows as 2D islands, as seen in the STM image in figure 3(a), and for coverages approaching 0.6 MLE the islands coalesce and form a wetting oxide layer (see figure 2(c)). The high-resolution STM image in figure 3(b) reveals the structural details of the $\sqrt{7}$ phase at the atomic scale, with a hexagonal lattice that consists of three bright protrusions per unit cell. The DFT calculations [15] have established a model of the $(\sqrt{7} \times \sqrt{7})$R19.1° structure (figures 3(c), (d)): it corresponds to a V_3O_9 oxide phase which contains identical pyramidal $O_4V{=}O$ building blocks (marked squares in figure 3(c)). Each pyramid (inset of figure 3(d)) has the vanadium atom (in green) in the centre, four bridging oxygen atoms (in red) in the basal plane and a vanadyl-type oxygen atom at the apex. The presence of the latter oxygen species in the $\sqrt{7}$ overlayer has been inferred from high-resolution electron energy loss spectroscopy (HREELS) spectra [15], which contain a characteristic loss at ∼130 meV due to the stretching vibrations of the vanadyl (V=O) groups. The pyramids are linked together via the four bridging oxygen atoms at the interface, which results in three VO_3 units per $\sqrt{7}$ unit cell, or in an overall V_3O_9 stoichiometry. Due to the fact that the basal oxygen atoms are shared with the rhodium substrate, the formal V_3O_9

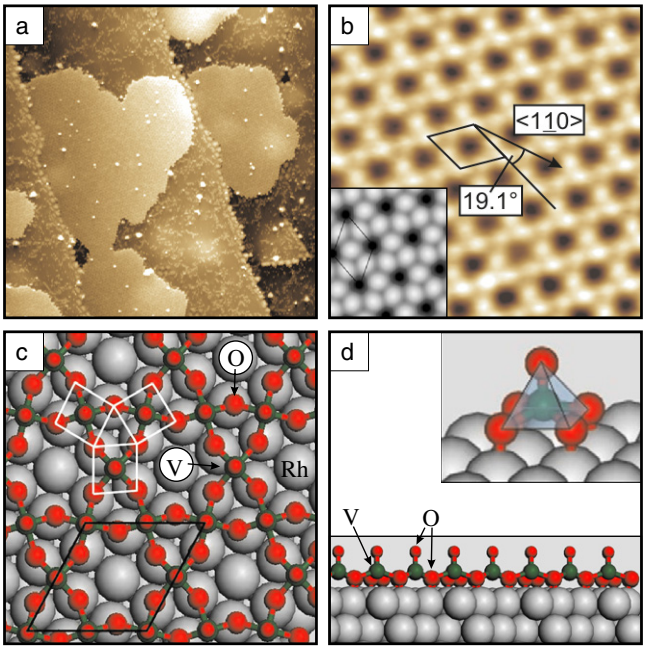

Figure 3. The ($\sqrt{7} \times \sqrt{7}$)R19.1° oxide phase. (a) Large-scale STM image (100 × 100 nm^2, $U = +2.0$ V, $I = 0.1$ nA) of 2D oxide islands on the Rh(111) surface. (b) High-resolution STM image (5 × 5 nm^2, $U = +0.75$ V, $I = 0.2$ nA). The ($\sqrt{7} \times \sqrt{7}$)R19.1° unit cell and the Rh(111) substrate direction are indicated. The inset shows a DFT-simulated STM image. (c) DFT model of the $\sqrt{7}$-V_3O_9 phase. The unit cell and structural units are indicated (V, green; O, red; Rh, grey). (d) Side view of the V_3O_9 model. The inset shows a detailed view of the pyramidal $O_4V{=}O$ unit.

stoichiometry is not incompatible with the maximum oxidation state of +5 of the vanadium atoms in the bulk V_2O_5 structure. The latter is constructed by similar square pyramidal $O_4V{=}O$ building blocks, but there they share edges and build double chains along the [010] direction, which are connected by their corners and form layers stacked in the [001] direction [16].

The structure model of the $\sqrt{7}$-V_3O_9 phase is confirmed by the good agreement between the experimental and simulated STM image (inset of figure 3(b)) and the calculated phonon spectrum, which reproduces the vanadyl stretching vibrations observed in the experiment [15]. Interestingly, for somewhat different preparation conditions, i.e. by PO of submonolayer vanadium coverages at $p(O_2) = 2 \times 10^{-7}$ mbar and $T = 400\,^{\circ}$C, another planar vanadium oxide phase with a ($\sqrt{13} \times \sqrt{13}$)R13.8° structure grows on the Rh(111) surface [15], which contains the same pyramidal $O_4V{=}O$ building blocks as the $\sqrt{7}$-phase. The DFT calculations [15] indicate that this phase has a V_6O_{18} stoichiometry, i.e. it contains six VO_3 units per unit cell, and that it is thermodynamically slightly more stable than the $\sqrt{7}$-phase. The formation of such highly oxidized vanadium oxide nanolayer phases with an oxidation state of the vanadium atoms close to +5 appears to be a more general phenomenon and is also observed on other metal substrates, such as Pd(111), for example. On the latter, a similar but tetragonal V–O coordination has been found for a (4 × 4)-V_5O_{14} wetting layer on the basis of DFT calculations [17].

The morphology and size of the $\sqrt{7}$-V_3O_9 islands can be controlled by varying the substrate temperature during oxide evaporation: due to the enhanced adatom mobility higher temperatures ($T \geqslant 400\,^{\circ}$C) result in large (lateral size $\geqslant$500 Å) and compact 2D oxide islands,

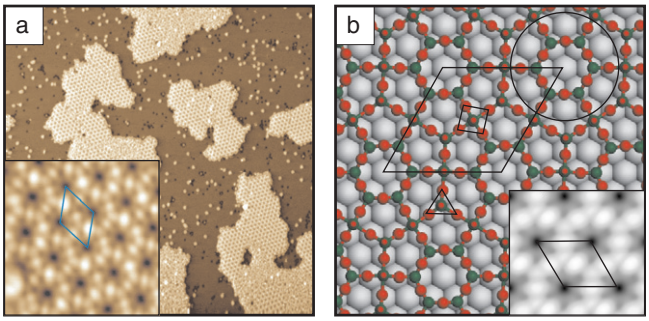

Figure 4. The (5 × 5) vanadium oxide phase. (a) Large-scale STM image (100 × 100 nm^2, $U = +2.0$ V, $I = 0.2$ nA). The inset shows a high-resolution STM image (4 × 4 nm^2, $U = +2.0$ V, $I = 0.2$ nA). (b) DFT model of the (5 × 5) $V_{11}O_{23}$ phase. The inset shows a DFT-simulated image.

whereas lower temperatures ($T \leqslant 250\,^{\circ}$C) yield smaller (typically $\leqslant$150 Å) and less regularly shaped islands [18]. Due to the higher perimeter to area ratio the smaller islands expose a larger number of low-coordination sites at their boundaries, which may exhibit an enhanced chemical reactivity. This has been demonstrated in a recent study of the CO oxidation reaction [18], which is promoted in the vicinity of the small $\sqrt{7}$-oxide islands.

Exposing the $\sqrt{7}$ or $\sqrt{13}$ phases to a reducing environment, e.g. by annealing in UHV or in a hydrogen atmosphere, results in the formation of various reduced 2D vanadium oxide phases, which involve mixed-valent oxides such as $V_{11}O_{23}$ and $V_{13}O_{21}$ and more reduced stoichiometric V_2O_3 and VO phases [12]. Instead of following in detail the transformation sequence of vanadium oxide nanolayers, which has been described in [12], we will focus here on the specific V–O building units constituting these structures. We start with the (5 × 5) phase, whose morphological and structural details are displayed in figure 4(a) and its inset. The STM image reveals well-ordered 2D oxide nanoislands; in between the islands bright spots are seen corresponding to V_6O_{12} oxide clusters, which will be addressed in more detail in section 4. The DFT model [12] of the (5 × 5) oxide phase is presented in figure 4(b) and corresponds to a $V_{11}O_{23}$ stoichiometry per unit cell. It also contains the pyramidal $O_4V{=}O$ units (marked square on the figure) present in the $\sqrt{7}$ and $\sqrt{13}$ structures, but here they are linked by other V–O building elements which involve hexagonal V_6O_{12} (circle) and trigonal $O_3V{=}O$ (triangle) units. The overall oxide stoichiometry is reduced from the VO_3 in the $\sqrt{7}$ phase to $VO_{2.09}$ in the (5 × 5) structure. The inset of figure 4(b) shows a simulated STM image as calculated from the DFT model, which is in excellent agreement with the experimental image and thus supports the structure model.

Upon further reduction the (5 × 5) phase transforms into a (5 × 3$\sqrt{3}$)-rect vanadium oxide structure [12]. The STM image in figure 5(a) illustrates the morphology of the (5 × 3$\sqrt{3}$)-rect phase, which forms well-ordered 2D islands of rectangular shape oriented along the $\langle 1\bar{1}0\rangle$ azimuthal directions of the Rh(111) surface. The (5 × 3$\sqrt{3}$)-rect unit cell is indicated in the high-resolution STM image (inset of figure 5(a)) and contains a bright maximum in the centre and dark holes in the corners. The corresponding DFT model is shown in figure 5(b) and contains again the pyramidal $O_4V{=}O$ (square on the figure) and the hexagonal V_6O_{12} (circle) units with a unit cell content of $V_{13}O_{21}$, yielding a formal $VO_{1.62}$ stoichiometry [12]. The simulated STM image (inset of figure 4(b)) reproduces very well the experimental one, which leaves little doubt about the correctness of the DFT model. Thus, it appears that the reduction of the $\sqrt{7}$ V_3O_9 layer proceeds via the removal of vanadyl groups. In the $\sqrt{7} \rightarrow$ (5 × 5) structure

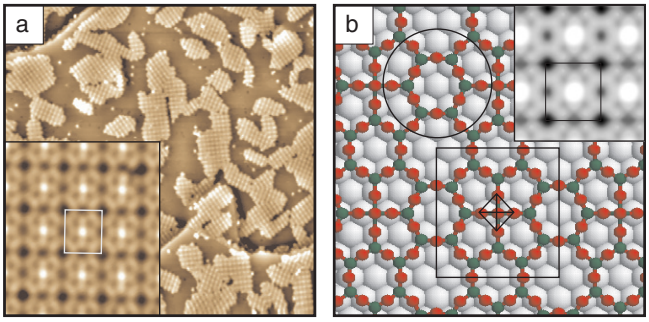

Figure 5. The $(5 \times 3\sqrt{3})$-rect vanadium oxide phase. (a) Large-scale STM image (100×100 nm^2, $U = +2.0$ V, $I = 0.1$ nA). The inset shows a high-resolution STM image (3.3×3.3 nm^2, $U = +2.0$ V, $I = 0.1$ nA). (b) DFT model of the $(5 \times 3\sqrt{3})$-rect $V_{13}O_{21}$ phase. The inset shows a DFT-simulated image.

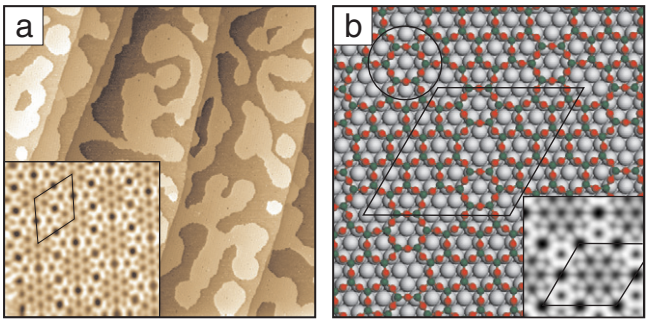

Figure 6. The (9×9) vanadium oxide phase. (a) Large-scale STM image (200×200 nm^2, $U = +2.0$ V, $I = 0.05$ nA). The inset shows a high-resolution STM image (6×6 nm^2, $U = +2.0$ V, $I = 0.1$ nA). (b) DFT model of the (9×9) $V_{36}O_{54}$ phase. The inset shows a DFT-simulated image.

transition two pyramidal $O_4V{=}O$ units are replaced by one trigonal $O_3V{=}O$ unit, containing one less bridging oxygen atom, and by one hexagonal V_6O_{12} unit, where the V=O group is absent. In the $(5 \times 3\sqrt{3})$-rect structure there is only one $O_4V{=}O$ unit left, containing the V=O group.

The removal of V=O groups is completed (as confirmed by HREELS) in the (9×9) vanadium oxide phase, which forms next in the reduction sequence [12]. The (9×9) oxide islands (figure 6(a)) display more rounded boundaries and less well-defined geometrical shapes, but the high-resolution STM image (inset of figure 6(a)) reveals a high degree of structural order within the islands. The corresponding DFT model is presented in figure 6(b) and involves hexagonal V_6O_{12} units (circles on the figure) and no pyramidal structures; the $V_{36}O_{54}$ content of the (9×9) unit cell corresponds to a V_2O_3 stoichiometry [12]. The DFT model was tested again by comparing the experimental and simulated STM images (inset of figure 6(b)): every single detail is reproduced in the simulation, and this lends strong support for the model. It is interesting to note that a wetting layer (2×2) phase with a V_2O_3 stoichiometry has been found on the Pd(111) substrate [19]. On the latter, the so-called surface- or s-V_2O_3 structure contains, however, simple hexagonal V–O units which share edges [11], whereas in the (9×9) phase on Rh(111) the V_6O_{12} hexagons share corner oxygen atoms.

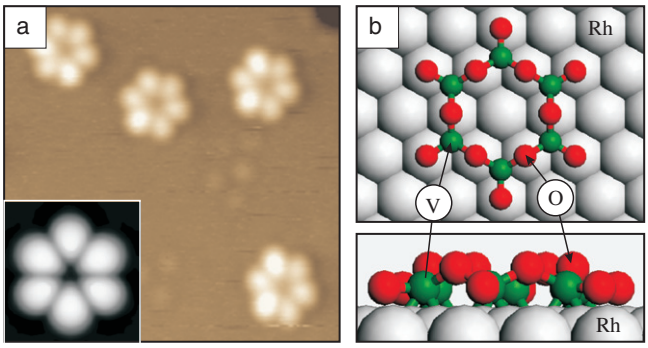

Figure 7. The V_6O_{12} cluster molecules on Rh(111). (a) STM image (6.3 × 6.3 nm^2, = +0.5 V, I = 0.1 nA). The inset shows a DFT-simulated image. (b) Relaxed DFT model geometry of the V_6O_{12} clusters on Rh(111) in top and side view.

4. Planar vanadium oxide clusters (0D oxide nanostructures)

Figure 2(a) shows a topographic STM image of a surface which has been prepared by evaporation of small submonolayer amounts ($\Theta < 0.2$ ML) of metallic vanadium onto the oxygen pre-dosed O-(2 × 1)Rh(111) surface and a subsequent flash to 250 °C in UHV. Bright objects identical in size and shape can be easily identified in this image. Atomically resolved STM images (figure 7(a)) reveal that each of these objects consists of six maxima arranged in a hexagon [20]. Their diameter D is 0.93 nm and their apparent height h is 0.12 nm. These oxide cluster molecules are therefore regarded as 0D nanostructures, since they are confined in all three spatial directions to <1 nm. DFT calculations [20] have established the stoichiometry and atomic structure of the star-like structures (figure 7(b)): each 'star' consists of six vanadium atoms which are coordinated to three rhodium substrate atoms. Six bridging oxygen atoms are positioned in between and slightly above the vanadium atoms. Six additional oxygen atoms are attached to each vanadium atom and are located on top of the rhodium substrate atoms. This yields a V_6O_{12} stoichiometry for each vanadium oxide star cluster with the formal oxidation state +4 for the vanadium atoms. A STM simulation based on this structure model is shown in the inset of figure 7(a). The simulation agrees excellently with the experimentally obtained STM image and thus confirms the structural model.

Theoretical analysis [20] has shown that the planar geometry of the star cluster is determined by the presence of the Rh(111) substrate. The observed planar geometry of the V_6O_{12} cluster is stabilized by 15.7 eV as a result of the bonding interaction to the Rh(111) surface. The latter value has been calculated by lifting the stars off the surface and relaxing the free-standing star in a vacuum. Vyboishchikov and Sauer [21] have studied free V_6O_{15} clusters and found a trigonal prism to be the most stable structure. In the computations the star-like V_6O_{12} cluster can be transformed to a V_6O_{15} cluster by attaching three double-bonded oxygen atoms to every second vanadium atom. The resulting V_6O_{15} cluster is unstable in the V–O–Rh phase diagram and cannot exist on the Rh(111) surface. This is a clear indication that the substrate plays a decisive role and is capable of modelling the shape and morphology of small nanoparticles.

The 0D cluster objects become mobile on the Rh(111) surface at elevated substrate temperatures. A thorough investigation of the diffusion process has shown that the stars move as entire clusters and perform a 2D random walk [20]. The height of the activation barrier for diffusion was evaluated to $E_d = 1.30 \pm 0.07$ eV. The diffusing oxide clusters may be condensed

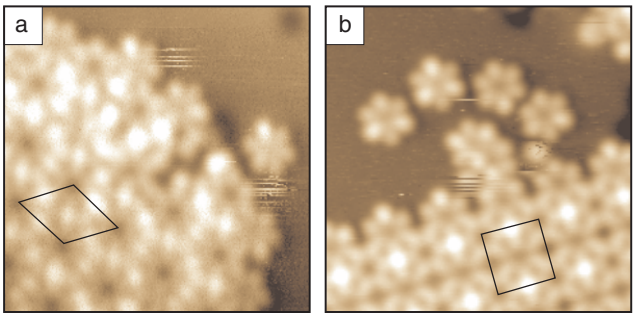

Figure 8. High-resolution STM images (7×7 nm^2, $U = +1.2$ V, $I = 0.1$ nA) of the boundary region of $(5 \times 5)V_{11}O_{23}$ (a) and $(5 \times 3\sqrt{3})$-rect $V_{13}O_{21}$ (b) islands displaying the agglomeration of V_6O_{12} clusters into the 2D oxide structures.

into two different 2D oxide structures with the help of a thermodynamically controlled self-assembly process. The oxygen partial pressure (or the related chemical potential of oxygen μ_O) is the experimental variable which controls this self-organization process and steers the condensation of the stars into one or the other structure [22]. For example, oxidizing conditions (high μ_O, $p_{O2} = 1 \times 10^{-8}$ mbar, $T \approx 250\,^\circ$C) lead to the condensation of V_6O_{12} clusters into the (5×5) 2D vanadium oxide phase. Figure 8(a) displays a high-resolution STM image, where a single star cluster is shown together with the (5×5) phase. The V_6O_{12} building units are not only present in the interior of (5×5) islands, as suggested by the DFT model (figure 4(b)), but also at the border of the (5×5) islands fragments of the star-like oxide clusters can be identified. The condensation of stars into the (5×5) phase increases the overall oxidation state of the vanadium atoms from +4 to +4.2 and can therefore be considered as an oxidation process. On the other hand, reducing ambient conditions (low μ_O, $p_{H2} = 1 \times 10^{-8}$ mbar, $T \approx 250\,^\circ$C) lead to the condensation into the $(5 \times 3\sqrt{3})$-rect oxide phase. Figure 8(b) visualizes this condensation process at the atomic scale in a snapshot: several oxide clusters are ready to attach to the border of a $(5 \times 3\sqrt{3})$-rect island. The vanadium atoms lower their oxidation state during the condensation into the rectangular phase (from +4 to +3.2), the condensation may thus be regarded as a direct visualization of a reduction process on the atomic scale.

The condensation of the star clusters into different 2D oxide phases depending on the chemical potential of oxygen μ_O may be understood with the help of the DFT-derived phase diagram [22]. Figure 9 presents an appropriate section of the V–O/Rh(111) surface phase diagram. The chemical potential of oxygen μ_O is plotted versus the concentration of vanadium atoms c_V at the surface. The latter is given in monolayers of vanadium atoms. The regions of stability of the respective oxide phases, depending on the chemical potential of oxygen and vanadium coverage, are indicated by the black bars. For a coverage of 0.45 MLE and a chemical potential of oxygen $\mu_O < 1.5$, the $(\sqrt{13} \times \sqrt{13})$R13° oxide phase is the most stable phase. With decreasing chemical potential the (5×5) phase and subsequently the $(5 \times 3\sqrt{3})$-rect phase become more stable. The V_6O_{12} oxide clusters are stable for low vanadium coverages in the grey shaded region of the phase stability diagram. In principle they can coexist with the (5×5) and the $(5 \times 3\sqrt{3})$-rect phase. By varying the chemical potential of oxygen the condensation of the star oxide clusters into the (5×5) or $(5\times3\sqrt{3})$-rect phase can be promoted: increasing the chemical potential (increasing the oxygen pressure) leads to the condensation into the (5×5) phase, whereas lowering the chemical potential (heating in UHV or H_2) results in the condensation of stars into the $(5 \times 3\sqrt{3})$-rect phase. Elevated substrate temperatures are required to overcome diffusion barriers and kinetic limitations.

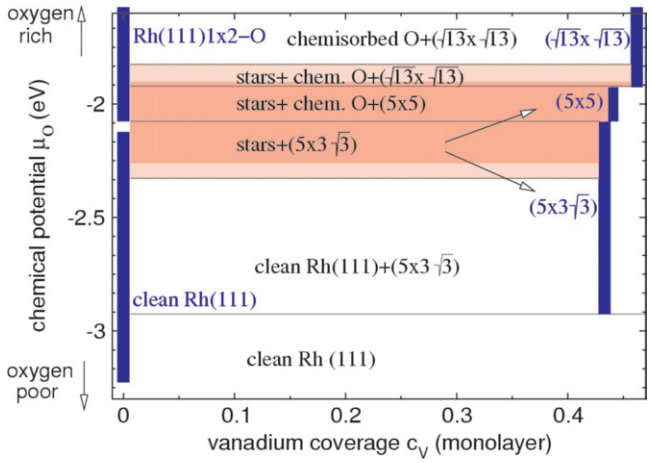

Figure 9. Section of the thermodynamic DFT phase diagram of vanadium oxide on Rh(111) in equilibrium with an oxygen reservoir which controls the chemical potential μ_O. Vertical black bars at the nominal vanadium coverage of each phase correspond to the μ_O region of stability. The arrows indicate the condensation of the V_6O_{12} clusters into the different 2D island structures under more oxidizing or reducing conditions.

5. 1D oxide nanostructures

Two different fabrication routes have been used in order to generate 1D oxide structures. First, diffusion and sticking anisotropy of the 0D oxide clusters on the Rh(111) surface has been exploited in order to aggregate them into 1D oxide structures on a flat Rh(111) surface. Figure 2(b) shows a STM image of a surface which was initially covered by individual oxide star clusters and was flashed to 250 °C in UHV afterwards. As a result, rectangular oxide islands are formed which are elongated along the $\langle 1\bar{1}0\rangle$ substrate directions. The high-resolution STM image of figure 10 reveals three oxide islands of the $(5 \times 3\sqrt{3})$-rect phase, which are oriented along the equivalent $[\bar{1}01]$, $[1\bar{1}0]$ and $[01\bar{1}]$ directions. The length of the islands extends up to 200 Å whereas their width is smaller than 20 Å. Thus, the oxide islands constitute 'quasi' one-dimensional structures with aspect ratios of up to 10. The origin of the anisotropic island shape can be ascribed to the interplay between diffusion and sticking anisotropy of the 0D oxide clusters. Theoretical investigations have shown that the diffusion barrier along the $\langle 1\bar{1}0\rangle$ directions is lower by 0.3 eV than along the $\langle 1\bar{2}1\rangle$ directions [23]. The oxide clusters will thus preferentially diffuse along the $\langle 1\bar{1}0\rangle$ directions until they hit an existing island (a critical nucleus) and will eventually stick to it. However, this mechanism alone will not lead to the observed island shapes since the islands should grow in all three $\langle 1\bar{1}0\rangle$ directions equally fast. In order to explain the morphology of the islands, the oxide star clusters have also to possess a sticking anisotropy. They have to attach more easily to the $\langle 1\bar{2}1\rangle$ island borders than to the island borders running along $\langle 1\bar{1}0\rangle$ directions. This combination of diffusion and sticking anisotropy can lead to the formation of 'quasi'-1D oxide structure.

The second fabrication route for 1D oxide structures makes use of stepped single-crystal metal surfaces, since these have been found suited for the growth of one-dimensional nanostructures such as metal nanowires [24, 25]. First attempts have been made to grow vanadium oxide nanostructures on a Rh(15,15,13) surface. Ideally, the terrace width on a Rh(15,15,13) surface is $d = 3.346$ nm. Atoms on the terraces show the symmetry of an fcc(111) surface and step atoms form (111) microfacets. Preliminary results from this study indicate that 1D oxide structures can indeed be formed on such a stepped metal surface [26].

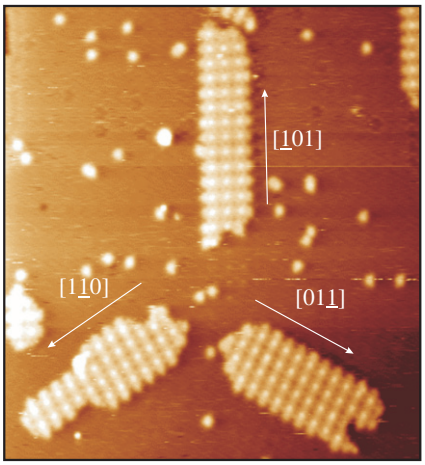

Figure 10. STM image (45×39 nm^2, $U = +2.0$ V, $I = 0.1$ nA) of a quasi 1D ($5 \times 3\sqrt{3}$)-rect $V_{13}O_{21}$ nanostructure. Three equivalent substrate directions are indicated on the figure.

6. 3D oxide nanoparticles

The 3D island morphology is the preferred growth mode of vanadium oxide on Rh(111) for oxide coverages above 1 MLE and substrate temperatures of around 400 °C (figure 1). Figure 11(a) displays the STM topography of the vanadium oxide islands for Θ_{ox} of 1.6 MLE: they exhibit truncated hexagonal shapes, slightly elongated along equivalent $\langle 11\bar{2}\rangle$ substrate directions, due to the anisotropy of the growth rate in this direction. The islands have lateral dimensions of up to 10 nm and a height of up to 2 nm, and are therefore considered as 3D nanoparticles. Larger-scale STM images (see figure 2(d)) show that the 3D vanadium oxide islands nucleate preferentially at the step edges, but occasionally they are observed to also nucleate on larger terraces (figure 11(a)). The STM image in figure 11(b) demonstrates that the 3D islands are terminated by an atomically flat and ordered surface, which exhibits a hexagonal structure, rotated by 30° with respect to the Rh(111) surface. The surface unit cell, as determined from the high-resolution STM image in figure 11(c), measures 4.9 ± 0.1 Å, which is very close to $\sqrt{3}$ times the Rh(111) lattice constant; the structure corresponds to a $(\sqrt{3} \times \sqrt{3})$R30° superstructure with respect to the substrate. The latter also persists for thicker vanadium oxide layers and is attributed to the (0001) plane of the bulk-type V_2O_3 phase with a corundum structure, which has a lattice constant of 4.9 Å [27]. Kresse *et al* [13] have investigated with DFT calculations the stability of different terminations of the V_2O_3(0001) surface over a wide range of oxygen chemical potentials and have found that the most stable one is not a bulk truncated surface but a surface layer containing vanadyl V=O groups in a (1×1) bulk unit cell. The vanadyl-terminated (1×1) surface structure is illustrated in the model of figure 11(d) and consists of an O_3 bulk-truncated V_2O_3(0001) surface which is terminated by a V=O layer. STM simulations [27] have shown that the maxima in the high-resolution STM image of figure 11(c) correspond to the V=O groups.

The substrate temperature during the deposition of the oxide is of critical importance for the fabrication of regularly shaped V_2O_3 nanoparticles with atomically well-ordered (0001) top facets. Higher temperatures (see highlighted region marked 3D in figure 1) are beneficial because of larger adatom diffusion lengths, which when exceeding the mean terrace width will result in the preferential nucleation of oxide islands at steps. At lower temperatures adatom diffusivities are lower, which leads to an enhanced condensation on the terraces. The resulting

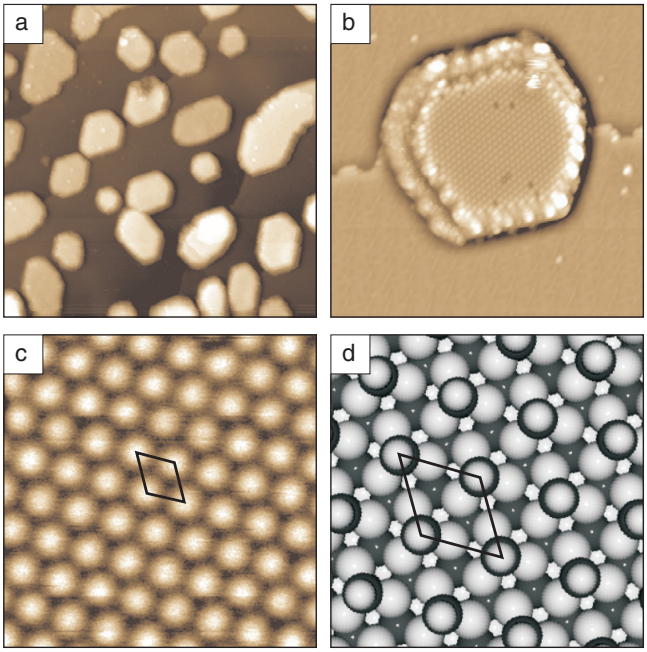

Figure 11. 3D V_2O_3 nanoparticles on Rh(111). (a) Large-scale STM image (100×100 nm^2, $U = +2.0$ V, $I = 0.1$ nA). (b) STM image (20×20 nm^2, $U = +2.0$ V, $I = 0.1$ nA) of a single V_2O_3 nanoparticle terminated by a (0001) surface plane. (c) High-resolution STM image (4×4 nm^2, $U = +0.2$ V, $I = 0.1$ nA) of the V_2O_3 (0001) surface with a unit cell indicated. (d) DFT model of the (1×1) V=O surface (vanadium, dark spheres; oxygen, bright spheres). A (1×1) unit cell is shown.

growth morphology is a rough polycrystalline V_2O_3 layer, which is poorly ordered on the long-range scale [12].

A further step towards the fabrication of ordered arrays of 3D oxide nanoislands is to grow V_2O_3 nanoparticles on stepped rhodium surfaces: by varying the miscut angle (i.e. the step density) one may hope to control the periodicity of the nanostructure. Further experiments will be necessary to see whether it will be possible to prepare periodic oxide nanostructures in such a way.

7. Synopsis

In this review we have described the formation of nanoscale oxide structures on a metal surface by reviewing results obtained in our laboratories on the growth of vanadium oxide overlayers on the group VIII metal Rh(111) surface. The vanadium oxide on Rh(111) system is prototypical for a (transition metal oxide overlayer)–(transition metal substrate) combination, which displays a rich diversity of structural phenomena. We show that vanadium oxide nanostructures can be formed on Rh(111) with morphologies ranging from quasi-zero-dimensional to three-dimensional and that the oxide growth can be tuned into a particular dimensionality by careful adjustment of experimental parameters. We describe the experimental growth procedure of PVD leading to the different vanadium oxide nanostructures and their structural characterization by atomically resolved STM images and *ab initio* DFT calculations. Although this review is concerned mainly with vanadium oxide nanostructures on

the Rh(111) surface, published work on vanadium oxides on Pd(111) and recent ongoing work on manganese oxides on Pd(100) in our group suggest that the phenomena described here are of a more general nature on oxide–metal systems.

The results presented in this review are a first step to characterizing the formation of metal-supported oxide nanostructures and understanding the underlying physical principles. However, the scientific and technological interest in this area is increasing rapidly, and more work on oxide nanostructures is expected in the near future. In the field of vacuum deposition of oxide nanostructured overlayers, the growth of oxides on nanopatterned surfaces will be an important topic. The use of vicinal metal surfaces as substrates is an obvious way to induce nanoscale structured overlayers, but substrate surfaces with regular strain patterns, which provide nucleation centres for promoting heterogeneous growth, may also be an interesting subject for further study. The process of self-assembly of oxide nanostructure arrays from molecular cluster units, which has been briefly mentioned in section 4, is interesting and deserves further scientific attention. Experimental and theoretical methods have now reached such a point that the elementary processes of surface diffusion and self-assembly may be elucidated with atomic precision. The field of oxide nanostructure research is wide open at present and we expect interesting progress in the years to come.

Acknowledgments

This work has been supported by the Austrian Research Funds through the Joint Research Programme 'Nanoscience on Surfaces'. JS acknowledges support from the Austrian Academy of sciences.

References

[1] Henrich V E and Cox P A 1994 *The Surface Science of Metal Oxides* (Cambridge: Cambridge University Press)
[2] Hermann K and Witko M 2001 *The Chemical Physics of Solid Surfaces: Oxide Surfaces* vol 9, ed D P Woodruff, (Amsterdam: Elsevier Science) chapter 4, p 136 and references therein
[3] Surnev S, Ramsey M G and Netzer F P 2003 *Prog. Surf. Sci.* **73** 117
[4] Kung H H 1989 *Transition Metal Oxides, Surface Chemistry and Catalysis* (New York: Elsevier)
[5] Weckhuysen B M and Keller D E 2003 *Catal. Today* **78** 25
[6] Stefanovich G, Pergament A and Stefanovich D 2000 *J. Phys.: Condens. Matter* **12** 8837
[7] Goward G R, Leroux F and Nazar L F 1998 *Electrochim. Acta* **43** 1307
[8] Patzke G R, Krumeich F and Nesper R 2002 *Angew. Chem. Int. Edn* **41** 2446
[9] Sakamoto J S and Dunn B 2002 *J. Electrochem. Soc.* **149** A26
[10] Wang H, Yi X, Chen S and Fu X 2005 *Sensors Actuators* A **122** 108
[11] Surnev S, Vitali L, Ramsey M G, Netzer F P, Kresse G and Hafner J 2000 *Phys. Rev.* B **61** 086102
[12] Schoiswohl J, Surnev S, Sock M, Eck S, Ramsey M G, Netzer F P and Kresse G 2005 *Phys. Rev.* B **71** 165437
[13] Kresse G, Surnev S, Schoiswohl J and Netzer F P 2004 *Surf. Sci.* **555** 118
[14] Surnev S, Kresse G, Ramsey M G and Netzer F P 2001 *Phys. Rev. Lett.* **87** 86102
[15] Schoiswohl J, Sock M, Eck S, Surnev S, Ramsey M G, Netzer F P and Kresse G 2004 *Phys. Rev.* B **69** 155403
[16] For a model of the V_2O_5 structure see e.g. Kämper A, Hahndorf I and Baerns M 2000 *Top. Catal.* **11/12** 77
[17] Surnev S, Sock M, Kresse G, Andersen J N, Ramsey M G and Netzer F P 2003 *J. Phys. Chem.* B **107** 4777
[18] Schoiswohl J, Eck S, Ramsey M G, Andersen J N, Surnev S and Netzer F P 2005 *Surf. Sci.* **580** 122
[19] Surnev S, Vitali L, Ramsey M G, Netzer F P, Kresse G and Hafner J 2000 *Phys. Rev.* B **61** 086102
[20] Schoiswohl J, Kresse G, Surnev S, Sock M, Ramsey M G and Netzer F P 2004 *Phys. Rev. Lett.* **92** 206103
[21] Vyboishchikov S F and Sauer J 2001 *J. Phys. Chem.* A **105** 8588
[22] Schoiswohl J, Surnev S, Sock M, Ramsey M G, Kresse G and Netzer F P 2004 *Angew. Chem. Int. Edn* **43** 5546
[23] Kresse G, private communication
[24] Gambardella P *et al* 2001 *Nature* **416** 301
[25] Gambardella P, Blanc M, Brune H, Kuhnke K and Kern K 2000 *Phys. Rev.* B **61** 2254
[26] Schoiswohl J, Surnev S and Netzer F P, unpublished
[27] Schoiswohl J, Sock M, Surnev S, Ramsey M G, Netzer F P, Kresse G and Andersen J N 2004 *Surf. Sci.* **555** 101